Featured in Physics

Direct Detection of Dark Photon Dark Matter Using Radio Telescopes

Haipeng An,[1,2,3,4,*] Shuailiang Ge,[3,5,†] Wen-Qing Guo,[6,7,‡] Xiaoyuan Huang,[6,7,§] Jia Liu,[5,3,‖] and Zhiyao Lu[5,¶]

[1]*Department of Physics, Tsinghua University, Beijing 100084, China*
[2]*Center for High Energy Physics, Tsinghua University, Beijing 100084, China*
[3]*Center for High Energy Physics, Peking University, Beijing 100871, China*
[4]*Frontier Science Center for Quantum Information, Beijing 100084, China*
[5]*School of Physics and State Key Laboratory of Nuclear Physics and Technology, Peking University, Beijing 100871, China*
[6]*Key Laboratory of Dark Matter and Space Astronomy, Purple Mountain Observatory, Chinese Academy of Sciences, Nanjing 210033, China*
[7]*School of Astronomy and Space Science, University of Science and Technology of China, Hefei, Anhui 230026, China*

(Received 19 July 2022; revised 30 November 2022; accepted 23 March 2023; published 2 May 2023)

Dark photons can be the ultralight dark matter candidate, interacting with Standard Model particles via kinetic mixing. We propose to search for ultralight dark photon dark matter (DPDM) through the local absorption at different radio telescopes. The local DPDM can induce harmonic oscillations of electrons inside the antenna of radio telescopes. It leads to a monochromatic radio signal and can be recorded by telescope receivers. Using the observation data from the FAST telescope, the upper limit on the kinetic mixing can already reach 10^{-12} for DPDM oscillation frequencies at 1–1.5 GHz, which is stronger than the cosmic microwave background constraint by about one order of magnitude. Furthermore, large-scale interferometric arrays like LOFAR and SKA1 telescopes can achieve extraordinary sensitivities for direct DPDM search from 10 MHz to 10 GHz.

DOI: 10.1103/PhysRevLett.130.181001

Introduction.—Ultralight bosons are attractive dark matter (DM) candidates, including QCD axions, axionlike particles, dark photons, etc. [1–3]. Dark photons mixed with photons through a marginal operator at low energy is one of the simplest extensions beyond the standard model of particle physics [4–9]. It can be a force mediator in the dark sector [1,10,11] or a DM candidate itself [12–15].

This Letter focuses on the dark photon dark matter (DPDM) with a mass $m_{A'}$, comparable to the energy of radio frequency photons (20 kHz–300 GHz). Ultralight DPDM can be produced through inflationary fluctuations [15–25], parametric resonances [26–31], cosmic strings [32], and the nonminimal coupling enhanced misalignment [13,14,33] with possible ghost instability [34,35]. Radio-frequency DPDM can be constrained indirectly by cosmic microwave background (CMB) spectrum distortion [14,36–38] and directly by haloscope experiments like TOKYO [39–42], FUNK [43], DM pathfinder and Dark E-field [44,45], SHUKET [46], WISPDMX [47], SQuAD [48], and recent experiments [49–52]. Axion haloscope search results [53–73] can be interpreted to DPDM limits [11,74], but some searches relying on the magnetic veto, e.g., RBF [75] and UF [76], cannot be translated into DPDM limits [11,77]. Proposals and future experiments to search for DPDM include plasma haloscopes [77,78], Dark E-field [45], DM-Radio [79–82], MADMAX [83], and solar radio observations [84,85].

One category of broadband haloscope experiments uses a dish reflector to look for dark photons [86–88]. The original proposal uses a spherical reflector to convert $A' \to \gamma$, and the monochromatic photons with energy $m_{A'}c^2$ are emitted perpendicular to the surface, thus focusing on the spherical center. This method has been applied to room-sized experiments [39–43,45,46], with variations using plane or parabolic reflectors or dipole antenna placed in a shielded room.

In this Letter, we propose to use existing and future radio telescopes to search for DPDM directly. With huge effective areas and great detectors, the sensitivities of large-scale radio telescopes can surpass current astrophysics bounds on radio-frequency DPDM by several orders of magnitude. We perform two types of studies: one exploits a single large dish antenna to convert dark photons into radio signals; the other uses antenna arrays forming interferometer pairs to receive radio signals, taking advantage of the long DPDM coherence.

Figure 1 summarizes our main results. The FAST data excludes the region surrounded by the solid red curve. The dashed red, blue, and brown curves show the projected sensitivities of FAST, LOFAR, and SKA1 [89] telescopes,

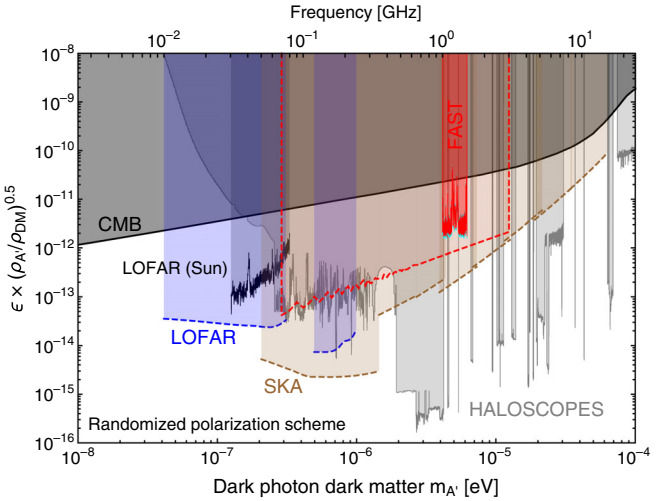

FIG. 1. Constraints and projected sensitivities on the kinetic mixing ϵ between DPDM and photon in the randomized polarization scheme. The 95% confidence level (C.L.) exclusion limit for DPDM using the FAST data is represented by the solid red curve with an $\mathcal{O}(10\%)$ uncertainty in cyan, while the dashed red curve indicates its future sensitivity projection. The blue and brown dashed curves show the future sensitivity projections of LOFAR and SKA1 interferometric array telescopes. The existing limits are from CMB constraints [14,36–38], solar radio observations [84,85], various haloscope searches [45–52], and axion experiments [53–73] translated to randomized polarization scheme [11,74].

assuming one-hour observation. For comparison, CMB and haloscopes constraints are shown by the black and gray shaded regions, respectively. The results show that large radio telescopes can play an essential and complementary role in DPDM searches.

Model.—We consider the dark photon Lagrangian

$$\mathcal{L} = -\frac{1}{4}F'_{\mu\nu}F'^{\mu\nu} + \frac{1}{2}m_{A'}^2 A'_\mu A'^\mu - \frac{1}{2}\epsilon F_{\mu\nu}F'^{\mu\nu}. \quad (1)$$

F' and F are dark photons and SM photons field strength; ϵ is the kinetic mixing. After appropriate rotation and redefinition, one can eliminate the kinetic mixing term and arrive at the interaction Lagrangian for A', the SM photon A, and the electromagnetic current $j^\mu_{\rm em}$,

$$\mathcal{L}_{\rm int} = e j^\mu_{\rm em}(A_\mu - \epsilon A'_\mu). \quad (2)$$

e is the electromagnetic coupling. Therefore, free electrons in telescope antennas will be accelerated by the DPDM electric field, $\mathbf{E}' = -\dot{\mathbf{A}}' - \nabla A'^0$, and then produce EM equivalent signals.

Since the local DM velocity is about $10^{-3}c$, where c is the speed of light, $\mathbf{E}'$ oscillates with a nearly monochromatic frequency, $f \approx m_{A'}/2\pi$. Therefore, radio telescopes will detect a monochromatic radio signal, broadening the center value of about 10^{-6}. The DPDM wavelength is about $10^3 c/f$, 10^3 times the same-frequency EM wavelength. Next, we analyze DPDM signals for the dipole antenna, dish antenna, and antenna arrays.

Response of the dipole antenna.—A dipole antenna usually comprises conductive elements like metal wires or rods. Considering a linear dipole antenna of length ℓ lying on the horizontal plane observing a radio signal from the zenith direction with frequency f, it will detect an oscillating electric field

$$E_{\rm EM} = E_0 \cos\psi \cos(2\pi f t - \mathbf{k}\cdot\mathbf{x}). \quad (3)$$

E_0 is the amplitude, $\mathbf{k}$ is the wave number, and ψ is the angle between the electric field and the antenna rod. ℓ is usually around half of the EM wavelength designed to detect. However, the DPDM wave number $\mathbf{k}'$ is about $\mathcal{O}(10^{-3})$ times smaller than $\mathbf{k}$ due to the small DM velocity. Therefore, according to Eq. (2), the antenna will register an equivalent electric field,

$$\begin{aligned} E^{\rm eqv}_{\rm EM} &= \epsilon E'_0 \cos\psi' \cos(2\pi f t - \mathbf{k}'\cdot\mathbf{x}), \\ &\simeq \epsilon E'_0 \cos\psi' \cos(2\pi f t). \end{aligned} \quad (4)$$

E'_0 is the amplitude of the dark electric field. ψ' is the angle between the dark electric field and the antenna rod.

Thus, typical dipole antennas respond to EM and DPDM fields differently, mainly by factors of ϵ and the polarization angle. Additionally, for the DPDM case, the antenna can always be seen as a *short* dipole antenna since $k'\ell \ll 1$ for proposed frequencies, modifying the antenna efficiency by an $\mathcal{O}(1)$ number. Therefore, for general dipole antennas, one can define a DPDM-induced equivalent EM flux density,

$$I^{\rm eqv}_{\rm dipole} \equiv \mathcal{C}_{\rm dipole}\epsilon^2\langle \mathbf{E}'^2\rangle = \mathcal{C}_{\rm dipole}\epsilon^2\rho_{\rm DM}. \quad (5)$$

$\rho_{\rm DM} = 0.3\ {\rm GeV/cm^3}$ is the conservative local DM energy density [90,91]. $\mathcal{C}_{\rm dipole}$ is an $\mathcal{O}(1)$ numerical factor. For telescopes like LOFAR and SKA1-Low, detailed antenna designs are needed to simulate the exact values of $\mathcal{C}_{\rm dipole}$, which is beyond the scope of the present work. Instead, we prove that $\mathcal{C}_{\rm dipole} \geq 1$ for the antenna with linear dipole configuration, showing that the DPDM signal gains enhancement over the EM signal in Sec. II of the Supplemental Material [92,93]. In this Letter, we *conservatively* assume $\mathcal{C}_{\rm dipole} = 1$ to estimate the potential sensitivity of LOFAR and SKA1-Low.

Response of the dish antenna.—Some large radio telescopes are constructed as dish antennas like FAST [94] or dish antenna arrays like MeerKAT [95] and SKA1-Mid [96]. A dish antenna usually comprises a parabolic reflector with the feed receiving reflected EM waves at the focus. Dishes are commonly made of metal plates. According to Eq. (2), DPDM causes free electrons on metal plates to

oscillate. Thus, each area unit can be seen as an oscillating dipole emitting EM waves with the same frequency as DPDM. Then, the feed signal is the integration over the dipole units. In Sec. I of the Supplemental Material [92], we show that the induced dipole with area dS is

$$d\mathbf{p} = 2\epsilon \mathbf{A}'_{\parallel} dS. \tag{6}$$

$\mathbf{A}'_{\parallel}$ is the projection of $\mathbf{A}'$ on dS. Then, the EM field at position $\mathbf{r}$ can be obtained by summing up area units,

$$\mathbf{B} = -\frac{\epsilon m_{A'}^2}{2\pi} \int dS_1 \mathbf{A}'_{\parallel} \times (\mathbf{r} - \mathbf{r}_1) \frac{e^{i m_{A'} |\mathbf{r}-\mathbf{r}_1|}}{|\mathbf{r} - \mathbf{r}_1|^2}. \tag{7}$$

The electric field $\mathbf{E}$ can be calculated using $\mathbf{B}$. EM phase at each dipole unit is determined by the DPDM wavelength, λ', different from the phase induced by parallel EM waves from distant stars. Therefore, the EM wave generated by DPDM will not focus on the antenna feed. For a single filled-aperture telescope like FAST, its diameter can be comparable to λ'. Thus, numerical simulation is necessary to calculate the induced EM flux into the feed. However, for dish antenna arrays like MeerKAT and SKA1-Mid, each dish's diameter is much smaller than λ'. Therefore, each dish's dipole units $d\mathbf{p}$ oscillate in phase.

Because of the continuous boundary condition for the electric field parallel to the metal surface, we have $\mathbf{E}_{\parallel} = \epsilon \mathbf{E}'_{\parallel}$ right outside the metal surface and the perpendicular component $|\mathbf{E}_{\perp}|/|\mathbf{E}_{\parallel}| \sim (f\lambda')^{-1} \approx 10^{-3}$. In Sec. I of the Supplemental Material [92], detailed calculation shows that the *reflected* EM wave propagates nearly perpendicular to the surface of the metal plate. Right on top of the reflector surface, its energy density can be estimated as $\epsilon^2 |\mathbf{E}'|^2 \cos^2\theta$, where θ is the angle between $\mathbf{E}'$ and the reflector plate.

Since the DPDM-induced EM wave is not focusing, its flux into the feed is much smaller than the total reflected flux. The parabolic antenna feed size is usually around the EM wavelength λ to optimize the absorption, so the reduction factor is roughly, $\lambda^2/\mathcal{A}$, the ratio between feed and reflector areas. Therefore, compared to the EM signal from distant sources, the DPDM-induced equivalent EM flux density can be written as

$$I_{\rm dish}^{\rm eqv} = \mathcal{C}_{\rm dish} \epsilon^2 \langle \mathbf{E}'^2 \rangle \times \frac{\lambda^2}{\mathcal{A}} = \mathcal{C}_{\rm dish} \epsilon^2 \rho_{\rm DM} \frac{\lambda^2}{\mathcal{A}}. \tag{8}$$

$\mathcal{C}_{\rm dish}$ is an $\mathcal{O}(1)$ numerical factor determined by the detailed antenna design. Numerical calculations of $\mathcal{C}_{\rm dish}$ are performed by averaging all possible A' polarization, denoted as the randomized polarization scheme. Results for FAST and SKA1-Mid are shown in Sec. I-C of the Supplemental Material [92].

Sensitivities of antenna arrays.—Radio telescopes using radio interferometry techniques can effectively enlarge the effective area and get better sensitivities on faint signals. The basic observation unit for radio interferometer array is the antenna pair [97]. Let $V_m(t)$ and $V_n(t)$ be the signal measured by the mth and nth antenna, then up to amplification factors, the pair's output signal is

$$r_{mn} = \langle V_m(t) V_n^*(t) \rangle. \tag{9}$$

$\langle \cdots \rangle$ means the time average. V_m and V_n can be seen as the voltage measured by antennas, proportional to the electric field. Therefore, the correlator r_{mn} is proportional to the EM flux density [97]. A telescope composed of N antennas has $N(N-1)/2$ independent pairs. The combined signal increases as $N(N-1)/2$, whereas the noise goes like $[N(N-1)/2]^{1/2}$. Thus, the signal-over-noise-ratio increases as $[N(N-1)/2]^{1/2} \approx N/\sqrt{2}$.

For normal EM signals, the minimum detectable spectral flux density of a radio telescope is

$$S_{\rm min} = \frac{\rm SEFD}{\eta_s \sqrt{n_{\rm pol} \mathcal{B} t_{\rm obs}}}. \tag{10}$$

$n_{\rm pol} = 2$ is the number of polarizations, η_s is the system efficiency, $t_{\rm obs}$ is the observation time, $\mathcal{B}$ is the bandwidth, and SEFD is the system equivalent (spectral) flux density,

$$\rm SEFD = \frac{2 k_B T_{sys}}{A_{eff}}. \tag{11}$$

$T_{\rm sys}$ is the antenna system temperature. $A_{\rm eff}$ is the antenna array' s effective area, increasing with the number of antennas N.

For the DPDM-induced signal, the correlation length is determined by its wavelength λ', beyond which the DPDM oscillation is out of phase; thus, the correlation is suppressed. For two antennas with distance d_{mn}, the correlation signal is suppressed by

$$\mathcal{S}_{mn} \approx \exp(-m_{A'}^2 v_0^2 d_{mn}^2/8). \tag{12}$$

$v_0 \approx 235$ km/s is the most probable velocity in the standard Halo model [98,99]. The detailed derivation uses truncated Maxwellian distribution, as shown in Sec. III of the Supplemental Material [92,100–104], consistent with Ref. [105].

Therefore, for an antenna array composed of N antennas, the DPDM-induced equivalent EM flux density is

$$I_{\rm array}^{\rm eqv} = \mathcal{S}_{\rm eff} I_{\rm single}^{\rm eqv}, \tag{13}$$

where

$$\mathcal{S}_{\rm eff} = \frac{2}{N(N-1)} \sum_{m=2}^{N} \sum_{n=1}^{m} \mathcal{S}_{mn}, \tag{14}$$

is the suppression factor. $I^{\rm eqv}_{\rm single}$ is the DPDM-induced EM flux density for an individual antenna, given by (5) for dipole antenna and (8) for dish antenna. For dipole array telescopes like LOFAR and SKA1-Low, the antennas first form stations, which are further organized into a large interferometer. Since each station's size is much smaller than λ', we neglect the suppression within a station. Therefore, the suppression factor becomes

$$\mathcal{S}_{\rm eff} = \frac{2}{N_{\rm stat}(N_{\rm stat}-1)} \sum_{m=2}^{N_{\rm stat}} \sum_{n=1}^{m} \mathcal{S}_{mn}. \tag{15}$$

$N_{\rm stat}$ is the number of stations. d_{mn} is the distance between the mth and nth stations.

Next, we will use the criterion

$$I^{\rm eqv}_{\rm array}/\mathcal{B} > S_{\rm min} \tag{16}$$

to estimate the projected sensitivities of LOFAR and SKA1 arrays for DPDM.

Constraints from FAST observation data.—FAST is currently the largest filled-aperture radio telescope. Its designed total bandwidth is from 70 MHz to 3 GHz with the current frequency resolution $\mathcal{B} = 7.63$ kHz and designed sensitivity $\mathrm{SEFD}^{-1} = 2000\ \mathrm{m}^2/\mathrm{K}$ [94,106]. During observation, a 300-meter aperture instantaneous paraboloid is formed to reflect and focus the EM wave into the feed. The DPDM-induced EM wave is not focusing and therefore suffers from the suppression factor, $\lambda^2/\mathcal{A}$; see Eq. (8). The simulation of the factor $\mathcal{C}$ for FAST at different frequencies is detailed in Sec. I-D of the Supplemental Material [92], from which we can calculate the DPDM-induced EM spectral flux density detected by FAST,

$$S^{\rm eqv}_{\rm FAST}(f) \equiv \frac{I^{\rm eqv}_{\rm FAST}}{\mathcal{B}} \approx 4.6\times 10^{-6}\epsilon^2 \frac{\mathcal{C}_{\rm FAST}(f)}{\mathcal{C}_{\rm FAST}(1\ \mathrm{GHz})} \frac{\mathrm{W}}{\mathrm{m^2\ Hz}}. \tag{17}$$

Requiring $S^{\rm eqv}_{\rm FAST} > S_{\rm min}$, we can calculate the sensitivity for the FAST telescope.

Apart from the simulation, we use the 19-beam L-band (1–1.5 GHz) observation data from FAST to set upper limits for DPDM. The observation was conducted on December 14, 2020, lasting 110 min. A time series of the signal is recorded for each frequency bin. We use the noise diode temperature to calibrate data and convert the signal to the EM spectral flux density by pre-measured antenna gain. DPDM induces a time-independent line spectrum signal, whereas most noise sources have transient features and can be reduced by data filtering processes [107]. Our data filtering process is detailed in Sec. IV of the Supplemental Material [14,92,107–110].

After data filtering, for each frequency bin i we obtain the average measured spectral flux density $\bar{O}_i$ and the statistic uncertainty $\sigma_{\bar{O}_i}$. We then use a polynomial function to locally model the background around the selected frequency bin i_0 with the help of its neighboring frequency bins. The systematic uncertainty is estimated by the data deviation to the background fit. Next, we assume a dark photon signal with the strength S existing at bin i_0, and a likelihood function L can be built between data and background function with S incorporated. Coefficients of the background polynomial function are treated as nuisance parameters. Following the likelihood-based statistical method [110], we compute the ratio λ_S between the conditional maximized-likelihood (e.g., only varying the nuisance parameters to maximize L while keeping S fixed) and the unconditional maximized-likelihood (e.g., varying both the nuisance parameters and S to maximize L). Then the test statistic, $-2\ln\lambda_S$, follows the half-χ^2 distribution [110]. Thus, we obtain the 95% C.L. upper limit, $S_{\rm lim}$, for a constant monochromatic signal, shown in Fig. 2.

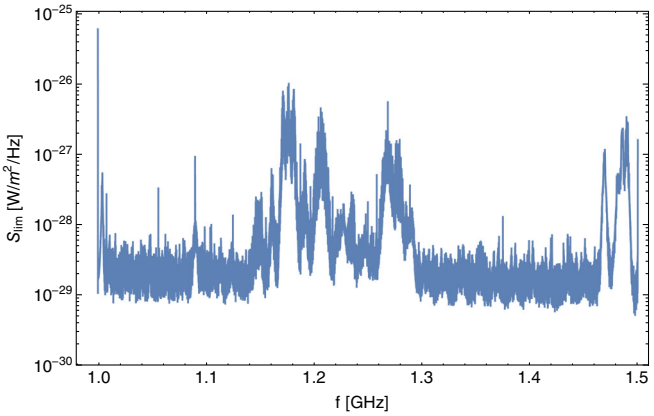

FIG. 2. Model-independent 95% C.L. upper limits on a constant monochromatic signal from FAST data in 1–1.5 GHz. It shows the strongest limit from the 19 beams at each frequency bin.

Upper limits on the mixing parameter ϵ are obtained via $S_{\rm lim} = S^{\rm eqv}_{\rm FAST}$. All 19 beams give similar constraints as expected. We choose the strongest limit among the 19 constraints for each frequency bin as the final result, shown in Fig. 1. The upper limits can reach $\epsilon \sim 10^{-12}$ in 1–1.5 GHz, about 1 order of magnitude better than the existing constraint from CMB measurement [14]. We emphasize that every single frequency between 1–1.5 GHz is constrained by the real data without any extrapolation. We also explore the rare case where the DPDM signal falls into two bins due to its broadening. The sensitivity calculation is similar but with a doubled data bandwidth. More details about the FAST original data, filtering processing, statistical methods, and numerical calculations are given in Sec. IV of the Supplemental Material [92].

Sensitivities of LOFAR and SKA1.—LOFAR is currently the largest radio telescope operating at the lowest frequencies (10–240 MHz), containing low-band antennas (LBAs) and high-band antennas (HBAs). LOFAR antennas are

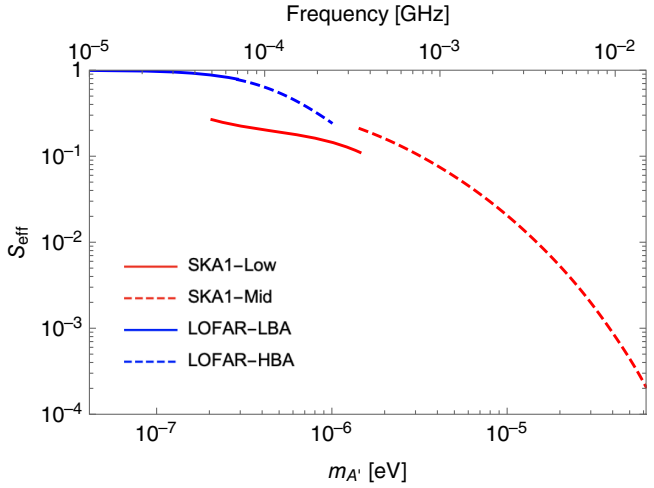

FIG. 3. Suppression factor $\mathcal{S}_{\rm eff}$ for SKA1 and LOFAR (only core stations) arrays in the interferometry.

grouped into 24 remote stations, each with a core size smaller than 2 km. DPDM wavelength within the LOFAR frequency range is 1.2–30 km. Therefore, we propose to use the core stations to search for DPDM. Station positions and relevant parameters can be found in Ref. [111]. The minimal frequency resolution, $\mathcal{B}_{\rm min}$, of LOFAR is about 700 Hz [111].

SKA1 continuously covers 50 MHz–20 GHz, including SKA1-Low and SKA1-Mid telescopes. SKA1-Low has 131 072 dipolelike antennas grouped into 512 stations, covering 50–350 MHz, with $\mathcal{B}_{\rm min} = 1$ kHz. Station positions and relevant parameters can be found in Refs. [112,113]. SKA1-Mid contains 133 SKA1 15-m diameter and 64 MeerKAT 13.5-m diam dish antennas. Therefore, its sensitivity on DPDM suffers from the additional suppression factor, $\lambda^2/\mathcal{A}$; see Eq. (8). SKA1-Mid has five bands, and the sensitivity and frequency range can be found in [114] and dish locations in [96]. SKA1-Mid achieves $\mathcal{B}_{\rm min} = 200$ Hz smaller than the DPDM natural width. Therefore, to calculate its DPDM sensitivity, we use the natural width, $\mathcal{B} = 10^{-6} f$.

The suppression factor $\mathcal{S}_{\rm eff}$ for DPDM signal using LOFAR and SKA1 arrays as interferometry are shown as the blue and red curves in Fig. 3, respectively. LOFAR is less suppressed than SKA1 due to lower frequency, thus longer DPDM coherent wavelength and smaller separation between stations.

Following Eq. (16), projected sensitivities on ϵ for LOFAR and SKA1 are shown in Fig. 1. LOFAR can cover a frequency down to 10 MHz, complementary to Haloscope searches. SKA1 shows competitive sensitivity for higher frequencies as a broadband search compared to resonant cavity searches.

Summary and outlook.—The radio telescopes' antennas can convert the DPDM field into an ordinary EM wave. We have analyzed the sensitivities of the commonly used dipole and parabolic dish antennas. We found that the parabolic one has a significant suppression factor for the DPDM-induced equivalent EM flux. For antenna arrays like LOFAR and SKA1, due to the sizable coherent length of DPDM, the interferometry technique in radio astronomy can enhance the sensitivity.

We have used FAST observational data to set limits for DPDM. The result is encouraging that for 1–1.5 GHz, the limit $\epsilon \sim 10^{-12}$ is 1 order of magnitude stronger than the CMB constraint. We have projected the sensitivities for FAST, LOFAR, and SKA1 telescopes and found that compared to room-sized haloscope experiments, they are competing and complementary in searching for DPDM directly.

The DPDM can directly interact with electrons through (2), inducing a signal in the feed. As detailed in the Supplemental Material [92], the signal induced from the reflector studied in this work is about 4 times larger than the direct feed signal, due to geometric reasons. However, the feed shape is complex, making it difficult to calculate the direct contribution accurately. The interference between the reflector and feed, along with the direct signal, may result in an $\mathcal{O}(10\%)$ uncertainty for the FAST limits in Fig. 1. Furthermore, the FAST sensitivity could be significantly improved if one can raise the feed to higher locations as shown in the Supplemental Material [92].

Dark photon mass can be generated through the Higgs mechanism or the Stückelberg mechanism. For the Higgsed case, the sub-keV dark photon is constrained to $\epsilon e_D < 10^{-14}$ by the stellar lifetime. e_D is the dark U(1) gauge coupling. This assumes the dark Higgs has a dark charge of one and a mass below keV [115]. Figure 1 demonstrates that the proposed radio search complements the stellar constraint for small e_D cases. For the Stückelberg case, the UV cutoff of the dark photon model is constrained by the weak gravity conjecture [116,117]. Although some production mechanisms for radio DPDM, like inflation-induced DPDM [15], are no longer favored by certain constraints [116], evading these constraints is possible by further developing the models [118]. Therefore, a radio DPDM search could provide insights into DPDM production mechanisms.

The authors would like to thank Peng Jiang, Yidong Xu, Jinglong Yu, Qiang Yuan, and Yanxi Zhang for helpful discussions. This work made use of the data from the five-hundred-meter aperture spherical radio telescope (FAST). FAST is a Chinese national mega-science facility, operated by National Astronomical Observatories, Chinese Academy of Sciences. The work of H. A. is supported in part by the National Key R&D Program of China under Grants No. 2021YFC2203100 and No. 2017YFA0402204, the NSFC under Grant No. 11975134, and the Tsinghua University Dushi Program No. 53120200422. The work of S. G. is supported by NSFC under Grant No. 12247147, the International Postdoctoral Exchange Fellowship Program,

and the Boya Postdoctoral Fellowship of Peking University. The work of X. H. is supported by the Chinese Academy of Sciences, and the Program for Innovative Talents and Entrepreneur in Jiangsu. The work of J. L. is supported by NSFC under Grant No. 12075005, 12235001 and by Peking University under startup Grant No. 7101502458.

*anhp@mail.tsinghua.edu.cn
†sge@pku.edu.cn
‡guowq@pmo.ac.cn
§xyhuang@pmo.ac.cn
‖jialiu@pku.edu.cn
¶2000011457@stu.pku.edu.cn

[1] R. Essig *et al.*, Working group report: New light weakly coupled particles, in *Proceedings of the 2013 Community Summer Study on the Future of U.S. Particle Physics: Snowmass on the Mississippi (CSS2013): Minneapolis, MN, USA, 2013* (2013), arXiv:1311.0029.
[2] M. Battaglieri *et al.*, US Cosmic Visions: New ideas in dark matter 2017: Community Report, in U.S. Cosmic Visions: New Ideas in Dark Matter College Park, MD, USA, 2017 (2017), arXiv:1707.04591.
[3] P. A. Zyla *et al.* (Particle Data Group), Review of particle physics, Prog. Theor. Exp. Phys. **2020**, 083C01 (2020).
[4] B. Holdom, Two U(1)'s and Epsilon charge shifts, Phys. Lett. **166B**, 196 (1986).
[5] K. R. Dienes, C. F. Kolda, and J. March-Russell, Kinetic mixing and the supersymmetric gauge hierarchy, Nucl. Phys. **B492**, 104 (1997).
[6] S. A. Abel and B. W. Schofield, Brane anti-brane kinetic mixing, millicharged particles and SUSY breaking, Nucl. Phys. **B685**, 150 (2004).
[7] S. A. Abel, J. Jaeckel, V. V. Khoze, and A. Ringwald, Illuminating the hidden sector of string theory by shining light through a magnetic field, Phys. Lett. B **666**, 66 (2008).
[8] S. A. Abel, M. D. Goodsell, J. Jaeckel, V. V. Khoze, and A. Ringwald, Kinetic mixing of the photon with hidden U(1)s in string phenomenology, J. High Energy Phys. 07 (2008) 124.
[9] M. Goodsell, J. Jaeckel, J. Redondo, and A. Ringwald, Naturally light hidden photons in LARGE volume string compactifications, J. High Energy Phys. 11 (2009) 027.
[10] M. Fabbrichesi, E. Gabrielli, and G. Lanfranchi, *The Physics of the Dark Photon* (Springer, Cham, 2021).
[11] A. Caputo, A. J. Millar, C. A. J. O'Hare, and E. Vitagliano, Dark photon limits: A handbook, Phys. Rev. D **104**, 095029 (2021).
[12] J. Redondo and M. Postma, Massive hidden photons as lukewarm dark matter, J. Cosmol. Astropart. Phys. 02 (2009) 005.
[13] A. E. Nelson and J. Scholtz, Dark light, dark matter and the misalignment mechanism, Phys. Rev. D **84**, 103501 (2011).
[14] P. Arias, D. Cadamuro, M. Goodsell, J. Jaeckel, J. Redondo, and A. Ringwald, WISPy cold dark matter, J. Cosmol. Astropart. Phys. 06 (2012) 013.
[15] P. W. Graham, J. Mardon, and S. Rajendran, Vector dark matter from inflationary fluctuations, Phys. Rev. D **93**, 103520 (2016).
[16] Y. Ema, K. Nakayama, and Y. Tang, Production of purely gravitational dark matter: The case of fermion and vector boson, J. High Energy Phys. 07 (2019) 060.
[17] E. W. Kolb and A. J. Long, Completely dark photons from gravitational particle production during the inflationary era, J. High Energy Phys. 03 (2021) 283.
[18] B. Salehian, M. A. Gorji, H. Firouzjahi, and S. Mukohyama, Vector dark matter production from inflation with symmetry breaking, Phys. Rev. D **103**, 063526 (2021).
[19] A. Ahmed, B. Grzadkowski, and A. Socha, Gravitational production of vector dark matter, J. High Energy Phys. 08 (2020) 059.
[20] Y. Nakai, R. Namba, and Z. Wang, Light dark photon dark matter from inflation, J. High Energy Phys. 12 (2020) 170.
[21] K. Nakayama and Y. Tang, Gravitational production of hidden photon dark matter in light of the XENON1T excess, Phys. Lett. B **811**, 135977 (2020).
[22] H. Firouzjahi, M. A. Gorji, S. Mukohyama, and B. Salehian, Dark photon dark matter from charged inflaton, J. High Energy Phys. 06 (2021) 050.
[23] M. Bastero-Gil, J. Santiago, L. Ubaldi, and R. Vega-Morales, Dark photon dark matter from a rolling inflaton, J. Cosmol. Astropart. Phys. 02 (2022) 015.
[24] H. Firouzjahi, M. A. Gorji, S. Mukohyama, and A. Talebian, Dark matter from entropy perturbations in curved field space, Phys. Rev. D **105**, 043501 (2022).
[25] T. Sato, F. Takahashi, and M. Yamada, Gravitational production of dark photon dark matter with mass generated by the Higgs mechanism, J. Cosmol. Astropart. Phys. 08 (2022) 022.
[26] R. T. Co, A. Pierce, Z. Zhang, and Y. Zhao, Dark photon dark matter produced by axion oscillations, Phys. Rev. D **99**, 075002 (2019).
[27] J. A. Dror, K. Harigaya, and V. Narayan, Parametric resonance production of ultralight vector dark matter, Phys. Rev. D **99**, 035036 (2019).
[28] M. Bastero-Gil, J. Santiago, L. Ubaldi, and R. Vega-Morales, Vector dark matter production at the end of inflation, J. Cosmol. Astropart. Phys. 04 (2019) 015.
[29] P. Agrawal, N. Kitajima, M. Reece, T. Sekiguchi, and F. Takahashi, Relic abundance of dark photon dark matter, Phys. Lett. B **801**, 135136 (2020).
[30] R. T. Co, K. Harigaya, and A. Pierce, Gravitational waves and dark photon dark matter from axion rotations, J. High Energy Phys. 12 (2021) 099.
[31] K. Nakayama and W. Yin, Hidden photon and axion dark matter from symmetry breaking, J. High Energy Phys. 10 (2021) 026.
[32] A. J. Long and L.-T. Wang, Dark photon dark matter from a network of cosmic strings, Phys. Rev. D **99**, 063529 (2019).
[33] G. Alonso-Álvarez, T. Hugle, and J. Jaeckel, Misalignment & Co.: (Pseudo-)scalar and vector dark matter with curvature couplings, J. Cosmol. Astropart. Phys. 02 (2020) 014.
[34] K. Nakayama, Vector coherent oscillation dark matter, J. Cosmol. Astropart. Phys. 10 (2019) 019,

[35] K. Nakayama, Constraint on vector coherent oscillation dark matter with kinetic function, J. Cosmol. Astropart. Phys. 08 (2020) 033.
[36] S. D. McDermott and S. J. Witte, Cosmological evolution of light dark photon dark matter, Phys. Rev. D **101**, 063030 (2020).
[37] A. Caputo, H. Liu, S. Mishra-Sharma, and J. T. Ruderman, Dark Photon Oscillations in Our Inhomogeneous Universe, Phys. Rev. Lett. **125**, 221303 (2020).
[38] S. J. Witte, S. Rosauro-Alcaraz, S. D. McDermott, and V. Poulin, Dark photon dark matter in the presence of inhomogeneous structure, J. High Energy Phys. 06 (2020) 132.
[39] J. Suzuki, Y. Inoue, T. Horie, and M. Minowa, Hidden photon CDM search at Tokyo, in *Proceedings of the 11th Patras Workshop on Axions, WIMPs and WISPs* (2015), pp. 145–148, arXiv:1509.00785.
[40] J. Suzuki, T. Horie, Y. Inoue, and M. Minowa, Experimental search for hidden photon CDM in the eV mass range with a dish antenna, J. Cosmol. Astropart. Phys. 09 (2015) 042.
[41] S. Knirck, T. Yamazaki, Y. Okesaku, S. Asai, T. Idehara, and T. Inada, First results from a hidden photon dark matter search in the meV sector using a plane-parabolic mirror system, J. Cosmol. Astropart. Phys. 11 (2018) 031.
[42] N. Tomita, S. Oguri, Y. Inoue, M. Minowa, T. Nagasaki, J. Suzuki, and O. Tajima, Search for hidden-photon cold dark matter using a K-band cryogenic receiver, J. Cosmol. Astropart. Phys. 09 (2020) 012.
[43] A. Andrianavalomahefa *et al.* (FUNK Experiment Collaboration), Limits from the FUNK experiment on the mixing strength of hidden-photon dark matter in the visible and near-ultraviolet wavelength range, Phys. Rev. D **102**, 042001 (2020).
[44] A. Phipps *et al.*, Exclusion limits on hidden-photon dark matter near 2 neV from a fixed-frequency superconducting lumped-element resonator, Springer Proc. Phys. **245**, 139 (2020).
[45] B. Godfrey *et al.*, Search for dark photon dark matter: Dark E field radio pilot experiment, Phys. Rev. D **104**, 012013 (2021).
[46] P. Brun, L. Chevalier, and C. Flouzat, Direct Searches for Hidden-Photon Dark Matter with the SHUKET Experiment, Phys. Rev. Lett. **122**, 201801 (2019).
[47] L. Hoang Nguyen, A. Lobanov, and D. Horns, First results from the WISPDMX radio frequency cavity searches for hidden photon dark matter, J. Cosmol. Astropart. Phys. 10 (2019) 014.
[48] A. V. Dixit, S. Chakram, K. He, A. Agrawal, R. K. Naik, D. I. Schuster, and A. Chou, Searching for Dark Matter with a Superconducting Qubit, Phys. Rev. Lett. **126**, 141302 (2021).
[49] R. Cervantes, C. Braggio, B. Giaccone, D. Frolov, A. Grassellino, R. Harnik, O. Melnychuk, R. Pilipenko, S. Posen, and A. Romanenko, Deepest sensitivity to wavelike dark photon dark matter with SRF cavities, arXiv:2208.03183.
[50] K. Ramanathan, N. Klimovich, R. Basu Thakur, B. H. Eom, H. G. LeDuc, S. Shu, A. D. Beyer, and P. K. Day, Wideband direct detection constraints on hidden photon dark matter with the QUALIPHIDE experiment, arXiv:2209.03419.
[51] R. Cervantes *et al.*, Search for 70 μeV Dark Photon Dark Matter with a Dielectrically Loaded Multiwavelength Microwave Cavity, Phys. Rev. Lett. **129**, 201301 (2022).
[52] S. Kotaka *et al.* (DOSUE-RR Collaboration), Search for Dark Photon Cold Dark Matter in the Mass Range 74–110 $\mu eV/c^2$ with a Cryogenic Millimeter-Wave Receiver, Phys. Rev. Lett. **130**, 071805 (2023).
[53] S. J. Asztalos *et al.* (ADMX Collaboration), A SQUID-Based Microwave Cavity Search for Dark-Matter Axions, Phys. Rev. Lett. **104**, 041301 (2010).
[54] N. Du, N. Force, R. Khatiwada, E. Lentz, R. Ottens *et al.* (ADMX Collaboration), A Search for Invisible Axion Dark Matter with the Axion Dark Matter Experiment, Phys. Rev. Lett. **120**, 151301 (2018).
[55] T. Braine, R. Cervantes, N. Crisosto, N. Du, S. Kimes *et al.* (ADMX Collaboration), Extended Search for the Invisible Axion with the Axion Dark Matter Experiment, Phys. Rev. Lett. **124**, 101303 (2020).
[56] C. Boutan, M. Jones, B. H. LaRoque, N. S. Oblath, R. Cervantes *et al.* (ADMX Collaboration), Piezoelectrically Tuned Multimode Cavity Search for Axion Dark Matter, Phys. Rev. Lett. **121**, 261302 (2018).
[57] L. Zhong, S. AlKenany, K. M. Backes, B. M. Brubaker, S. B. Cahn *et al.* (HAYSTAC Collaboration), Results from phase 1 of the HAYSTAC microwave cavity axion experiment, Phys. Rev. D **97**, 092001 (2018).
[58] K. M. Backes *et al.* (HAYSTAC Collaboration), A quantum-enhanced search for dark matter axions, Nature (London) **590**, 238 (2021).
[59] D. Alesini, C. Braggio, G. Carugno, N. Crescini, D. DAgostino *et al.*, Search for invisible axion dark matter of mass $m_a = 43$ μeV with the QUAX–$a\gamma$ experiment, Phys. Rev. D **103**, 102004 (2021).
[60] S. Lee, S. Ahn, J. Choi, B. R. Ko, and Y. K. Semertzidis, Axion Dark Matter Search around 6.7 μeV, Phys. Rev. Lett. **124**, 101802 (2020).
[61] J. Jeong, S. W. Youn, S. Bae, J. Kim, T. Seong, J. E. Kim, and Y. K. Semertzidis, Search for Invisible Axion Dark Matter with a Multiple-Cell Haloscope, Phys. Rev. Lett. **125**, 221302 (2020).
[62] O. Kwon, D. Lee, W. Chung, D. Ahn, H. S. Byun *et al.* (CAPP Collaboration), First Results from an Axion Haloscope at CAPP around 10.7 μeV, Phys. Rev. Lett. **126**, 191802 (2021).
[63] C. Bartram *et al.* (ADMX Collaboration), Search for Invisible Axion Dark Matter in the 3.3–4.2 μeV Mass Range, Phys. Rev. Lett. **127**, 261803 (2021).
[64] N. Crisosto, P. Sikivie, N. S. Sullivan, D. B. Tanner, J. Yang, and G. Rybka, ADMX SLIC: Results from a Superconducting *LC* Circuit Investigating Cold Axions, Phys. Rev. Lett. **124**, 241101 (2020).
[65] Y. Lee, B. Yang, H. Yoon, M. Ahn, H. Park, B. Min, D. L. Kim, and J. Yoo, Searching for Invisible Axion Dark Matter with an 18 T Magnet Haloscope, Phys. Rev. Lett. **128**, 241805 (2022).
[66] J. Kim *et al.*, Near-Quantum-Noise Axion Dark Matter Search at CAPP around 9.5 μeV, Phys. Rev. Lett. **130**, 091602 (2023).

[67] A. K. Yi *et al.*, Axion Dark Matter Search around 4.55 μeV with Dine-Fischler-Srednicki-Zhitnitskii Sensitivity, Phys. Rev. Lett. **130**, 071002 (2023).

[68] C. M. Adair *et al.*, Search for dark matter axions with CAST-CAPP, Nat. Commun. **13**, 6180 (2022).

[69] M. J. Jewell *et al.* (HAYSTAC Collaboration), New results from HAYSTAC's phase II operation with a squeezed state receiver, arXiv:2301.09721.

[70] A. P. Quiskamp, B. T. McAllister, P. Altin, E. N. Ivanov, M. Goryachev, and M. E. Tobar, Direct search for dark matter axions excluding ALP cogenesis in the 63- to 67-μeV range with the ORGAN experiment, Sci. Adv. **8**, abq3765 (2022).

[71] D. Alesini, C. Braggio, G. Carugno, N. Crescini, D. DAgostino *et al.*, Galactic axions search with a superconducting resonant cavity, Phys. Rev. D **99**, 101101(R) (2019).

[72] D. Alesini, D. Babusci, C. Braggio, G. Carugno, N. Crescini *et al.*, Search for Galactic axions with a high-Q dielectric cavity, Phys. Rev. D **106**, 052007 (2022).

[73] H. Chang, J. Y. Chang, Y. C. Chang, Y. H. Chang, Y. H. Chang *et al.* (TASEH Collaboration), First Results from the Taiwan Axion Search Experiment with a Haloscope at 19.6 μeV, Phys. Rev. Lett. **129**, 111802 (2022).

[74] C. O'Hare, cajohare/dark photon limits, https://cajohare.github.io/AxionLimits/docs/dp.html (2020).

[75] S. De Panfilis, A. C. Melissinos, B. E. Moskowitz, J. T. Rogers, Y. K. Semertzidis, W. U. Wuensch, H. J. Halama, A. G. Prodell, W. B. Fowler, and F. A. Nezrick, Limits on the Abundance and Coupling of Cosmic Axions at $4.5 < m_a < 5.0$ μev, Phys. Rev. Lett. **59**, 839 (1987).

[76] C. Hagmann, P. Sikivie, N. S. Sullivan, and D. B. Tanner, Results from a search for cosmic axions, Phys. Rev. D **42**, 1297 (1990).

[77] G. B. Gelmini, A. J. Millar, V. Takhistov, and E. Vitagliano, Probing dark photons with plasma haloscopes, Phys. Rev. D **102**, 043003 (2020).

[78] M. Lawson, A. J. Millar, M. Pancaldi, E. Vitagliano, and F. Wilczek, Tunable Axion Plasma Haloscopes, Phys. Rev. Lett. **123**, 141802 (2019).

[79] S. R. Parker, J. G. Hartnett, R. G. Povey, and M. E. Tobar, Cryogenic resonant microwave cavity searches for hidden sector photons, Phys. Rev. D **88**, 112004 (2013).

[80] S. Chaudhuri, P. W. Graham, K. Irwin, J. Mardon, S. Rajendran, and Y. Zhao, Radio for hidden-photon dark matter detection, Phys. Rev. D **92**, 075012 (2015).

[81] M. Silva-Feaver, S. Chaudhuri, H.-M. Cho, C. Dawson, P. Graham, K. Irwin, S. Kuenstner, D. Li, J. Mardon, H. Moseley, R. Mule, A. Phipps, S. Rajendran, Z. Steffen, and B. Young, Design overview of DM radio pathfinder experiment, IEEE Trans. Appl. Supercond. **27**, 1 (2017).

[82] S. Chaudhuri, K. Irwin, P. W. Graham, and J. Mardon, Optimal impedance matching and quantum limits of electromagnetic axion and hidden-photon dark matter searches, arXiv:1803.01627.

[83] A. Caldwell, G. Dvali, B. Majorovits, A. Millar, G. Raffelt, J. Redondo, O. Reimann, F. Simon, and F. Steffen (MADMAX Working Group), Dielectric Haloscopes: A New Way to Detect Axion Dark Matter, Phys. Rev. Lett. **118**, 091801 (2017).

[84] H. An, F. P. Huang, J. Liu, and W. Xue, Radio-Frequency Dark Photon Dark Matter Across the Sun, Phys. Rev. Lett. **126**, 181102 (2021).

[85] H. An, X. Chen, S. Ge, J. Liu, and Y. Luo, Searching for ultralight dark matter conversion in solar corona using LOFAR data, arXiv:2301.03622.

[86] D. Horns, J. Jaeckel, A. Lindner, A. Lobanov, J. Redondo, and A. Ringwald, Searching for WISPy cold dark matter with a dish antenna, J. Cosmol. Astropart. Phys. 04 (2013) 016.

[87] J. Jaeckel and J. Redondo, Resonant to broadband searches for cold dark matter consisting of weakly interacting slim particles, Phys. Rev. D **88**, 115002 (2013).

[88] J. Jaeckel and S. Knirck, Directional resolution of dish antenna experiments to search for WISPy dark matter, J. Cosmol. Astropart. Phys. 01 (2016) 005.

[89] The SKA telescope will be constructed in two phases: SKA1 is being designed now; SKA2 is planned to follow, but not yet fully defined. Therefore, in this Letter, we only calculate the SKA1 sensitivity for DPDM.

[90] P. F. de Salas, K. Malhan, K. Freese, K. Hattori, and M. Valluri, On the estimation of the local dark matter density using the rotation curve of the Milky Way, J. Cosmol. Astropart. Phys. 10 (2019) 037.

[91] P. F. de Salas and A. Widmark, Dark matter local density determination: Recent observations and future prospects, Rep. Prog. Phys. **84**, 104901 (2021).

[92] See Supplemental Material at http://link.aps.org/supplemental/10.1103/PhysRevLett.130.181001 for more details.

[93] R. Chatterjee, *Antenna Theory and Practice* (New Age International, New Delhi, 1996).

[94] R. Nan, D. Li, C. Jin, Q. Wang, L. Zhu, W. Zhu, H. Zhang, Y. Yue, and L. Qian, The five-hundred aperture spherical radio telescope (FAST) project, Int. J. Mod. Phys. D **20**, 989 (2011).

[95] MeerKAT Science: On the pathway to the SKA, 2016.

[96] SKA Collaboration, Ska1-mid physical configuration coordinates, Document number: SKA-TEL-INSA-0000537, 2015.

[97] A. Thompson, J. Moran, and G. Swenson Jr, *Interferometry and Synthesis in Radio Astronomy (Second Edition)* (Wiley-VCH Verlag GmbH&Co. KGaA, New York, 2004).

[98] P. J. McMillan and J. J. Binney, The uncertainty in Galactic parameters, Mon. Not. R. Astron. Soc. **402**, 934 (2010).

[99] J. Bovy, D. W. Hogg, and H.-W. Rix, Galactic masers and the Milky Way circular velocity, Astrophys. J. **704**, 1704 (2009).

[100] J. W. Foster, N. L. Rodd, and B. R. Safdi, Revealing the dark matter halo with axion direct detection, Phys. Rev. D **97**, 123006 (2018).

[101] C. A. J. O'Hare, C. McCabe, N. W. Evans, G. C. Myeong, and V. Belokurov, Dark matter hurricane: Measuring the S1 stream with dark matter detectors, Phys. Rev. D **98**, 103006 (2018).

[102] N. W. Evans, C. A. J. O'Hare, and C. McCabe, Refinement of the standard halo model for dark matter searches in light of the Gaia Sausage, Phys. Rev. D **99**, 023012 (2019).

[103] C. A. J. O'Hare, N. W. Evans, C. McCabe, G. C. Myeong, and V. Belokurov, Velocity substructure from Gaia and direct searches for dark matter, Phys. Rev. D **101**, 023006 (2020).
[104] J. W. Foster, Y. Kahn, R. Nguyen, N. L. Rodd, and B. R. Safdi, Dark matter interferometry, Phys. Rev. D **103**, 076018 (2021).
[105] A. Derevianko, Detecting dark-matter waves with a network of precision-measurement tools, Phys. Rev. A **97**, 042506 (2018).
[106] L. Qian, R. Yao, J. Sun, J. Xu, Z. Pan, and P. Jiang, FAST: Its scientific achievements and prospects, Innovation **1**, 100053 (2020).
[107] J. W. Foster, S. J. Witte, M. Lawson, T. Linden, V. Gajjar, C. Weniger, and B. R. Safdi, Extraterrestrial Axion Search with the Breakthrough Listen Galactic Center Survey, Phys. Rev. Lett. **129**, 251102 (2022).
[108] P. Jiang *et al.*, Commissioning progress of the FAST, Sci. China Phys. Mech. Astron. **62**, 959502 (2019).
[109] P. Jiang *et al.* (FAST Collaboration), The fundamental performance of FAST with 19-beam receiver at L band, Res. Astron. Astrophys. **20**, 064 (2020).
[110] G. Cowan, K. Cranmer, E. Gross, and O. Vitells, Asymptotic formulae for likelihood-based tests of new physics, Eur. Phys. J. C **71**, 1554 (2011); **73**, 2501(E) (2013).
[111] M. P. van Haarlem *et al.*, LOFAR: The LOw-Frequency ARray, Astron. Astrophys. **556**, A2 (2013).
[112] SKA Collaboration, Ska1-low configuration, Document number: SKA-SCI-LOW-001, 2015.
[113] SKA Collaboration, Ska1 system baselinev2 description, Document number: SKA-TEL-SKO-0000308, 2015.
[114] SKA Collaboration, Ska1: Design baseline description, Document number: SKA-TEL-SKO-0001075, 2019.
[115] H. An, M. Pospelov, and J. Pradler, Dark Matter Detectors as Dark Photon Helioscopes, Phys. Rev. Lett. **111**, 041302 (2013).
[116] M. Reece, Photon masses in the landscape and the swampland, J. High Energy Phys. 07 (2019) 181.
[117] M. Montero, J. B. Muñoz, and G. Obied, Swampland bounds on dark sectors, J. High Energy Phys. 11 (2022) 121.
[118] N. Craig and I. Garcia Garcia, Rescuing massive photons from the swampland, J. High Energy Phys. 11 (2018) 067.